AD-A116 770 ARMY ENGINEER TOPOGRAPHIC LABS FORT BELVOIR VA F/G 9/2
APPLYING PHOTOGRAMMETRY TO REAL TIME COLLECTION OF DIGITAL IMAG--ETC(U)
NOV 81 M A CROMBIE, W A BARACAT
UNCLASSIFIED ETL-0275 NL

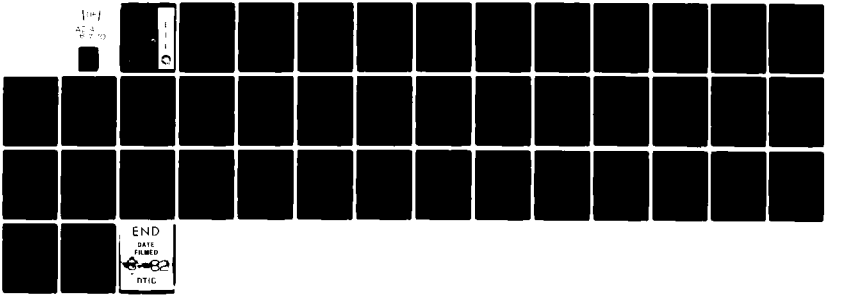

END
DATE FILMED
8-82
DTIC

ETL-0275

Applying photogrammetry to real time collection of digital image data

Michael A. Crombie

William A. Baracat

NOVEMBER 1981

U.S. ARMY CORPS OF ENGINEERS
ENGINEER TOPOGRAPHIC LABORATORIES
FORT BELVOIR, VIRGINIA 22060

E T L

U.S. ARMY ENGINEER TOPOGRAPHIC LABORATORIES ETL

UNCLASSIFIED

SECURITY CLASSIFICATION OF THIS PAGE (When Data Entered)

REPORT DOCUMENTATION PAGE		READ INSTRUCTIONS BEFORE COMPLETING FORM
1. REPORT NUMBER ETL-0275	2. GOVT ACCESSION NO. AD-A116 770	3. RECIPIENT'S CATALOG NUMBER
4. TITLE (and Subtitle) APPLYING PHOTOGRAMMETRY TO REAL TIME COLLECTION OF DIGITAL IMAGE DATA		5. TYPE OF REPORT & PERIOD COVERED Research Note 6. PERFORMING ORG. REPORT NUMBER
7. AUTHOR(s) William A. Baracat Michael A. Crombie		8. CONTRACT OR GRANT NUMBER(s)
9. PERFORMING ORGANIZATION NAME AND ADDRESS U.S. Army Engineer Topographic Laboratories Fort Belvoir, VA 22060		10. PROGRAM ELEMENT, PROJECT, TASK AREA & WORK UNIT NUMBERS 4A762707A855
11. CONTROLLING OFFICE NAME AND ADDRESS U.S. Army Engineer Topographic Laboratories Fort Belvoir, VA 22060		12. REPORT DATE November 1981 13. NUMBER OF PAGES 38
14. MONITORING AGENCY NAME & ADDRESS(if different from Controlling Office)		15. SECURITY CLASS. (of this report) Unclassified 15a. DECLASSIFICATION/DOWNGRADING SCHEDULE
16. DISTRIBUTION STATEMENT (of this Report) Approved for Public Release; Distribution Unlimited.		
17. DISTRIBUTION STATEMENT (of the abstract entered in Block 20, if different from Report)		
18. SUPPLEMENTARY NOTES		
19. KEY WORDS (Continue on reverse side if necessary and identify by block number) Digital Image Data Real Time Terrain Mapping x-parallax Epipolar Correlation Supplementary Attitude Stabilization y-parallax		
20. ABSTRACT (Continue on reverse side if necessary and identify by block number) The practicality of converting digital and stereo image data into terrain elevation data in real time is investigated. Results indicated that the real time collection of elevation data using epipolar correlation methods is not feasible. It is shown that real time mensuration of y-parallax can be used as a means to help maintain a desired relative orientation in a variety of digital collection system.		

DD FORM 1 JAN 73 1473 EDITION OF 1 NOV 65 IS OBSOLETE

UNCLASSIFIED

SECURITY CLASSIFICATION OF THIS PAGE (When Data Entered)

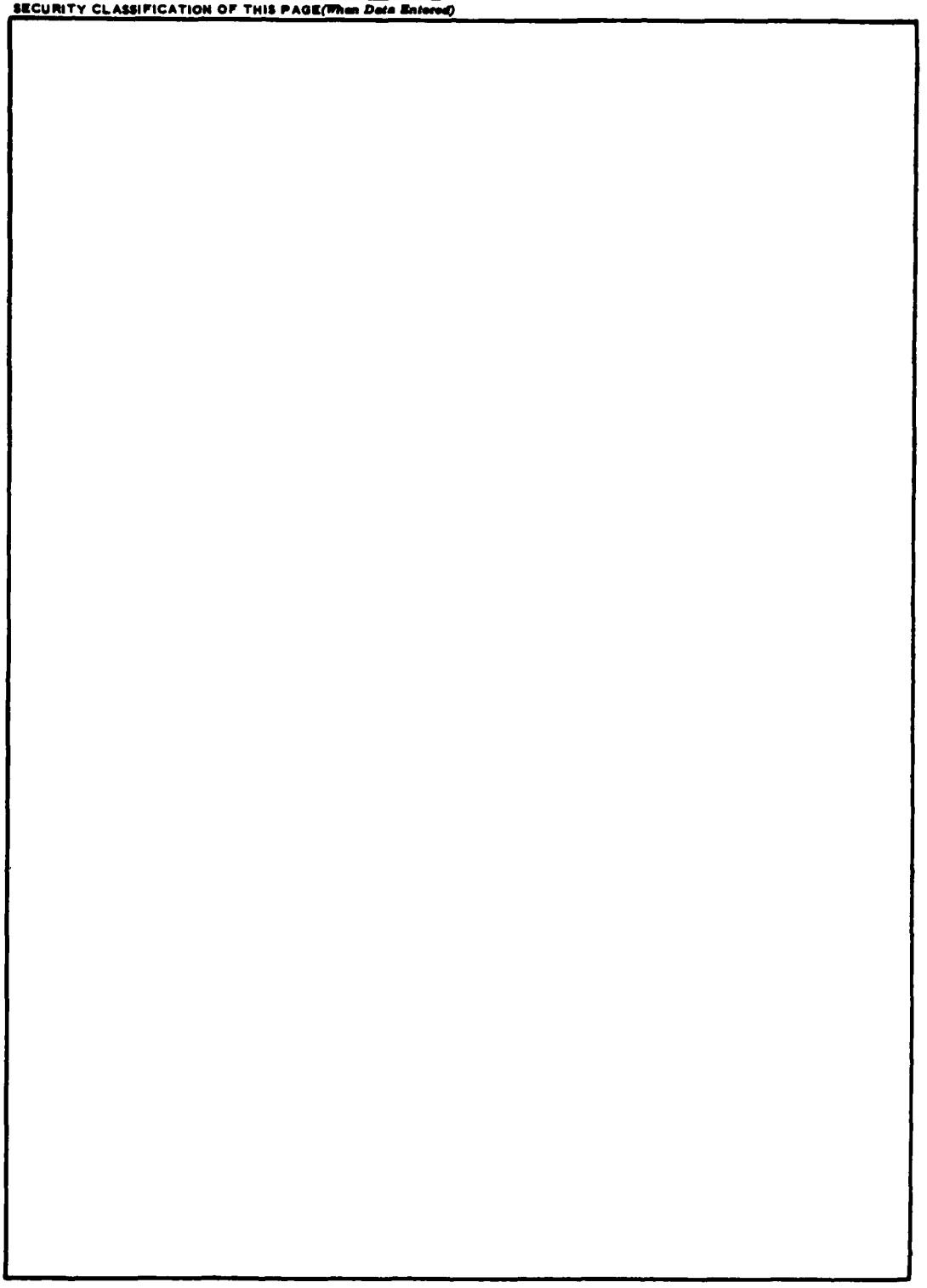

PREFACE

This study was conducted under DA project 4A762707A55, Task B, Work Unit 00016, "Digital Correlation Studies."

The study was done during the summer of 1980 under the supervision of Mr. D.E. Howell, Chief, Information Sciences Division; and Mr. L.A. Gambino, Director, Computer Sciences Laboratory.

The computer implementation and analysis was performed by Mr. William A. Baracat, a graduate co–op student from Virginia Polytechnic Institute.

COL Daniel L. Lycan, CE and COL Edward K. Wintz, CE were Commanders and Directors and Mr. Robert P. Macchia was Technical Director of the Engineer Topographic Laboratories during the study and report preparation.

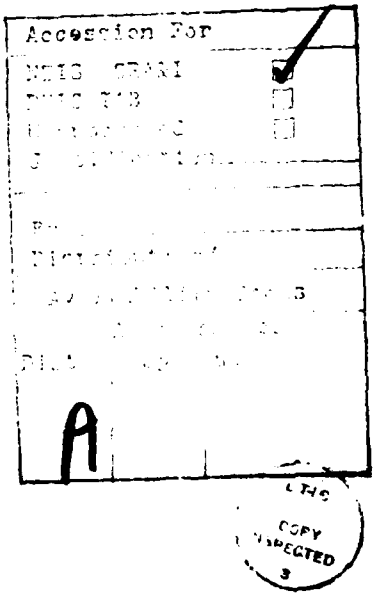

CONTENTS

ILLUSTRATIONS

TABLES

APPLYING PHOTOGRAMMETRY TO REAL TIME COLLECTION OF DIGITAL IMAGE DATA

INTRODUCTION

The purpose of the research was to explore the possibility of using photogrammetric techniques as an aid in real time attitude stabilization, cruise missile control, and terrain mapping when image data is collected digitally rather than by conventional film methods. The fundamental concepts of x–parallax and y–parallax were used to measure terrain heights and system attitude deviations, respectively. Epipolar line correlation was used to measure x–parallax and the coplanarity relation was used to control y–parallax. Two digital image sensing modes were considered. In the first mode, data was collected in a manner similar to a conventional strip camera; in the second mode, data was collected in a manner similar to a conventional chimney-type panoramic camera. Tests were conducted with digitized stereo image data. The tests were designed to evaluate three measures of similarity in epipolar image matching and to evaluate y-parallax as a measure of relative attitude control.

It was assumed in this study that the digital imaging system was composed of a solid state linear array of detectors configured in a vehicle such that the image data was collected in a manner amenable to efficient stereo processing. It was intended that the sensed data be used to compute elevation data in real time for mapping purposes or to control a cruise missile in flight. Results indicate that a more practical use would be to produce stereo image data ready for direct input to existing stereo compilation equipment.

DESCRIPTION OF TWO DIGITAL SENSOR CONFIGURATIONS

Two digital stereo image sensor systems are described in this section primarily to help describe the role of two photogrammetric operations in determining ground elevations and in supporting attitude control. The two imaging systems are described in a general way; a more thorough geometric description is presented in the appendixes.

Model 1 ■ This system, where two camera frames are locked together, is the simpler of the two. In each, a linear array of solid state detectors is arranged in the focal plane so that the extent of the array is perpendicular to the flight path. This system provides continuous stereo coverage of a narrow band of terrain along the vehicle ground track. If the relative attitude of the camera complex remains constant over time, then the Jth detector pair (one from each linear array) produces a stream of epipolar data that can be used to compute elevation data either in real time or later using conventional compilation practices (see appendix E for a description of epipolar correlation). Note that in this model the Jth detector defines the Jth epipolar plane.

The relative attitude of the camera complex pertains to the relative attitude of the forward camera at time T and the aft camera at time $T + DT + \delta_{TJ}$ when the two imaging rays defined by the Jth detectors intersect the ground and, if all is well, one another. The time interval DT corresponds to a fixed elevation and δ_T pertains to time deviations about DT owing to the undulating terrain. The relative geometry should remain constant for all δ_T. Deviations from the desired relative geometry can be detected by measuring y-parallax.

The y-parallax, including its measurement, is described in appendix D. It is a measure of the lack of coplanarity of the baseline and the estimated imaging rays. If the output from the forward array is held in the x-parallax calculation, then any y-parallax – significantly different from zero – can be attributed to a change in relative orientation. The y-parallax can be measured for several of the detectors over the linear format for input to a Kalman filter. The output of the filter would be corrections to the relative orientation parameters at time (T = DT/2).

Model 2 ■ Model 2 differs from Model 1 in that the camera frames are not locked together. Each linear array of detectors is free to scan. The arrays are arranged in the focal plane so that the extent of the arrays is parallel to the flight path. This system provides continuous stereo coverage of a wide band of terrain along the vehicle ground track. Continuous ground coverage along the track can be obtained by designing the exposure interval so that digital stereo pairs either abut or overlap.

The cameras scan across the flight path to acquire ground coverage while at the same time they yaw about their optical axes so that the detector output from both cameras for the same scan angle will be corresponding epipolar data. If both cameras scan in unison then epipolar data are collected at the same instant. If the two cameras scan in opposite directions to cancel vehicle rotational effects then epipolar data are collected at different times. If the two cameras scan in unison, then the y–parallax calculations discussed for Model 1 apply. The major difference here is that the output of the Kalman filter would be used to correct relative orientation parameters at time T, the time of scan. If the two cameras scan in opposite directions, then the output of the filter would be used to correct the relative orientation parameters at a time midway between the two exposures.

NUMERICAL EXPERIMENTS

The digitized image used for this experiment is stored in the DIAL (Digital Image Analysis Laboratory) system[1] and is described in a previous ETL research note.[2] The digitized image is a subimage taken from an exposure of rugged terrain. The essential features of the digitized model are

EXPOSURE DATA

Camera Type:	Vertical frame
Focal Length:	6 inches (15.2 cm)
Scale:	1:48,000

[1] Lawrence A. Gambino and Bryce L. Schrock, "An Experimental Digital Interactive Facility," *Computer*, Vol. 10, No. 8, August 1977, pp. 22–28.

[2] Michael A. Crombie, *Stereo Analysis of a Specific Digital Model Sampled From Aerial Imagery*, U.S. Army Engineer Topographic Laboratories, Fort Belvoir, VA, ETL–0072, September 1976, AD–A033 567.

DIGITAL DATA

Image Dimension:	2048 x 2048
Grayshades:	256
Aperture Size:	34.5 μm (micrometers)
Sample and Line Spacing:	24 μm

Three numerical experiments were performed. The first was an autocorrelation test designed to evaluate three basic measures of similarity (see appendix E) when used to register corresponding epipolar data. The second experiment was an evaluation of the same measures of similarity, but in a stereo mode. The third experiment was a demonstration of how the lack of correspondence between lines of image data can be detected and measured by estimating y–parallax.

Ordinarily, there would not be match errors in an autocorrelation process. However, because the computed autocorrelation function is seldom symmetric about the true match point, the estimation procedure does induce small errors. The averages of the errors for all three measures of similarity were less than 0.01 of the sample spacing. A set of M regularly spaced correlation values was calculated at and about the trial match point (in this test, the trial match point is the exact match point), and the maximal point was determined by regarding the correlation function as quadratic. If the largest (or smallest in the case of XDY) of the M discrete correlation values occurred at either end of the set, then a warning flag was activated. There were no warnings for the absolute difference measure (XDY) or for the linear correlation coefficient measure (RXY). Eleven lines of image data were processed in the auto-correlation mode. The matching window sizes were varied from 11 to 101 samples in steps of 10. The correlation function was estimated with 5 correlation values per match and with 7 values per match. The results are presented in tables 1 and 2. The dashed values pertain to standard errors less than 0.01 sample spacing.

An attempt was made to match all possible points. The number of trial matches per line is $N = 2050 - M - L$, where L is the window size. Thus, the number of trial matches per line is varied from 1942 to 2034. The units of table 1 are sample spacings, whereas the units of table 2 are counts.

TABLE 1. Standard Error of Mismatch for Autocorrelation of Linear Arrays

Window Size	RXY M=5	RXY M=7	SXY M=5	SXY M=7	XDY M=5	XDY M=7
11	.08	.08	.27	.40	.03	.03
21	.05	.05	.21	.28	.02	.02
31	.03	.03	.17	.23	.01	.01
41	.02	.02	.16	.20	.01	.01
51	.02	.02	.14	.17	.01	.01
61	.02	.02	.13	.15	.01	.01
71	.01	.01	.12	.13	—	—
81	.01	.01	.11	.12	—	—
91	.01	.01	.10	.11	—	—
101	.01	.01	.09	.09	—	—

TABLE 2. Warning Statistics for SXY

Window Size	W_N 5	W_N 7	σ_{WN} 5	σ_{WN} 7
11	95	79	21	18
21	47	42	16	19
31	32	29	15	17
41	22	20	13	14
51	13	14	9	11
61	10	10	7	10
71	7	8	5	8
81	4	5	5	6
91	3	4	4	5
101	2	2	3	4

The purpose of the autocorrelation experiment was to evaluate the performance of the three correlation measures under ideal conditions. The purpose of the stereo experiment was to evaluate the same measures under more realistic conditions. The stereo process was initiated at line 1527. The most recent results from an area matching exercise were used to shape the dependent line.[3] The epipolar matching process proceeded by first calculating parallax shifts for line 1527 and then using the derived results to shape the dependent member of the epipolar pair of lines associated with line 1528. The process continued in this manner and was halted at line 1542. The following statistics were recorded for each of the 16 lines:

u_s : Average x–parallax shift

σ_s : Standard deviation of the computed x–parallax

W_N : Number of warnings

The following statistics were recorded for lines 1527, 1532, 1537, and 1542:

Δu : Average x–parallax error

σ_{Δ_u} : Standard deviation of x–parallax error

The error data was generated by comparing coordinate values derived in the epipolar process to those derived by area correlation. There were 390 such comparisons made over the four lines. The results are presented in table 3.

It should be noted that line pairs of data used above are not exactly epipolar line pairs. This fact explains part of the error increase as more lines are processed. The same is true in the third experiment where y–parallax is used to detect and estimate an epipolar line shift.

[3] F. Raye Norvelle, "Interactive Digital Correlation Techniques for Automatic Compilation of Elevation Data," U.S. Army Engineer Topographic Laboratories, Fort Belvoir, VA, ETL-0272, October 1981.

TABLE 3. Statistical History of Stereo Epipolar Matching.

Line No.		1527	1528	1529	1530	1531	1532	1533	1534	1535	1536	1537	1538	1539	1540	1541	1542
RXY	u_s	.09	.05	−.01	.03	.09	−.16	.02	.07	.20	.07	−.14	.00	.14	.11	.10	.04
	σ_s	.18	.25	.14	.24	.18	.21	.25	.30	.60	.41	.59	.49	.41	.42	.53	.40
	W_N	0	0	0	0	0	0	0	0	8	0	24	127	59	69	55	93
	Δu	−.08					−.18					−.31					−.44
	$\sigma_{\Delta u}$	.31					1.50					2.47					4.24
SXY	u_s	.09	.06	−.00	.04	.10	−.13	.04	.20	.40	.23	−.07	.26	.11	.19	−.27	−.03
	σ_s	.18	.26	.17	.29	.26	.28	.37	.58	.71	.63	.50	.69	.75	.71	.99	.31
	W_N	0	0	0	0	0	2	6	1	136	12	323	266	124	13	60	150
	Δu	−.06					−.21					−.87					−1.16
	$\sigma_{\Delta u}$	.36					1.59					3.06					5.43
XDY	u_s	.23	−.04	.08	−.09	.19	−.27	.16	−.09	−.26	.16	.08	.10	.09	−.09	−.08	.04
	σ_s	.41	.45	.53	.74	.79	.99	.91	.85	.87	.99	.77	.72	.97	1.12	1.20	.94
	W_N	0	0	2	38	25	74	269	227	548	104	233	379	304	208	157	443
	Δu	−.18					−.05					−.01					−.09
	$\sigma_{\Delta u}$	.51					2.76					4.59					6.65

If the instantaneous relative orientation parameters as described in appendix D are known, then any image point selected on the left (or right) image uniquely determines corresponding epipolar lines. Since the defining epipolar plane is a member of the family of planes specified by the base line, any pair of points selected on the two lines will satisfy the coplanarity condition. However, if a point on the second image is selected on a neighboring epipolar line, the resultant ray will not be in the defined epipolar plane and a y–parallax error will be the result. In table 4, y–parallax errors are considered as a function of line error, and x–parallax errors, for a pair of lines selected in the following way. A line of data on the left image was selected and regarded as an epipolar line. Forty points (25 pixel spacing) were selected along this line, and the corresponding epipolar line was defined by the 40 match points determined in the area-matching experiment referenced above. Errors were introduced, and y–parallax, expressed as ΔY_{p2} in appendix D, was computed and tabulated.

TABLE 4. y – Parallax Errors.

x – Parallax Errors	LINE ERRORS							
	0	10	20	30	40	60	80	100
0	0.3	10.3	20.3	30.3	40.3	60.3	80.3	100.3
25	0.6	10.6	20.6	30.6	40.6	60.6	80.6	100.6
50	0.9	10.9	20.9	30.9	40.9	60.9	80.9	100.9
75	1.2	11.2	21.2	31.2	41.2	61.2	81.2	101.2

The entries in table 4 are average y–parallax errors expressed in sample spacings. That the two lines are not exactly epipolar pairs is indicated by the increase in y–parallax as x–parallax errors increase. The y–parallax deviation from the ideal y–parallax value (induced line error) ranges from 0.3 sample spacing to 1.2 sample spacing as x–parallax error ranges from 0 to 75 sample spacing. This bias holds over the entire range of induced errors. The standard deviation for each entry is 0.7 sample spacing. The range of deviations for each entry of table 4 was estimated from the error results and found to be $(\Delta Y - 0.8) \leq R \leq (\Delta Y + 0.2)$ for all cases.

DISCUSSION

The fact that XDY performed better than RXY in the autocorrelation of epipolar data was not surprising since a similar result was achieved under another autocorrelation test.[4] The relatively poor performance of the covariance function SXY was not too surprising since there is no gaurantee that the exact match point will produce the largest covariance value. Generally it will, but there are many cases, especially when small windows are used in busy areas, where SXY will not produce a maximum at the true match point. This fact is highlighted by the large standard deviations in table 1 and by the large number of warnings in table 2. Warnings were given whenever the largest of the measures (SXY) occurred at the end of a set of M measures. There were no warnings for XDY or for RXY in the autocorrelation tests.

The measure of similarity RXY proved to be superior to both XDY and SXY in the stereo tests (see table 3) and SXY was shown to perform better than XDY. This result is consistent with previously referenced studies (see 2 and 3) and with results taken from a passpoint study.[5] The measure RXY is not affected by an additive or multiplicative luminance difference between images of the same scene. The measure SXY is unaffected by an additive difference, whereas XDY is affected by both distortions.

The primary reason for considering SXY over RXY, and XDY over both, is ease of computation. The computing time for the similarity measures is the largest single item in the compilation computing time budget and any worthwhile savings should be exploited. The additive and multiplicative effects in RXY or the additive effects in SXY can be accounted for in one pass of the data; however, two passes would be necessary to compute either of the modifications of XDY given below:

$$XDYA = 1/N \sum_{i=1}^{N} \left| (Xi - \bar{X}) - (Yi - \bar{Y}) \right|$$

[4] Michael A. Crombie, Philip G. Lem, and Thomas A. Hay, *Single Photo Analysis of Sampled Aerial Imagery*, U.S. Army Engineer Topographic Laboratories, Fort Belvoir, VA, ETL-RN-74-10, August 1974, AD A012 176.

[5] Michael A. Crombie, *Semi-automatic Passpoint Determination Using Digital Techniques*, U.S. Army Engineer Topographic Laboratories, Fort Belvoir, VA, ETL-0051, December 1975, AD-A026 082.

$$XDYAM = 1/N \sum_{i=1}^{N} \left| (Xi - \bar{X}) / \sigma_x - (Yi - \bar{Y}) / \sigma_y \right|$$

Tests should be conducted to determine whether either of these measures is superior to RXY in stereo tests.

One purpose of this study was to explore the possibility of real time calculation of terrain elevation data. Although the data used for the tests were not exact epipolar data, the results definitely show that it would be extremely risky to rely on a totally automated, unmonitored correlation process. The process described in this report traveled across only 16 epipolar lines (about 65 feet), yet a glance at table 3 shows the process coming apart. Processing refinements, such as using XDYA as XDYAM, or employing a modified area matching concept with epipolar data[6] might produce acceptable results, but it is doubtful. Consideration would have to be given to obscuration due to clouds and to loss of correlation due to water, featureless terrain, etc. Since most of these nuisances have not been addressed satisfactority in a controlled environment, it is highly unlikely that the real time collection of terrain elevation data can be realized in the near future.

However, photogrammetric relations can be used to aid in data acquisition for subsequent and efficient data processing. It is not necessary that all y-parallax be removed before compilation. For example, the data used for the experiments in this study contain some y-parallax, yet the digitized images can be viewed quite satisfactorily in anaglyph form, and conventional digital correlation processes were used to compute elevation data.[7,8] Near epipolar data was obtained by transferring principal points between the image transparencies and then placing the transparencies in the scanner so that the approximate base line projection was parallel to the scan axis. The epipolar notion is discussed in appendix D and shown in figure 1.

---

[6] Frank Scarano and Gerry Brumm, "A Digital Elevation Collection System," *Photogrammetric Engineering and Remote Sensing*, Vol. XLII, No. 4, April 1976.

[7] Michael A. Crombie, *Stereo Analysis of a Specific Digital Model Sampled From Aerial Imagery*, U.S. Army Engineer Topographic Laboratories, Fort Belvoir, VA, ETL-0072, September 1976, AD-A033 567.

[8] F. Raye Norvelle, "Interactive Digital Correlation Techniques for Automatic Compilation of Elevation Data," U.S. Army Engineer Topographic Laboratories, Fort Belvoir, VA, to be published.

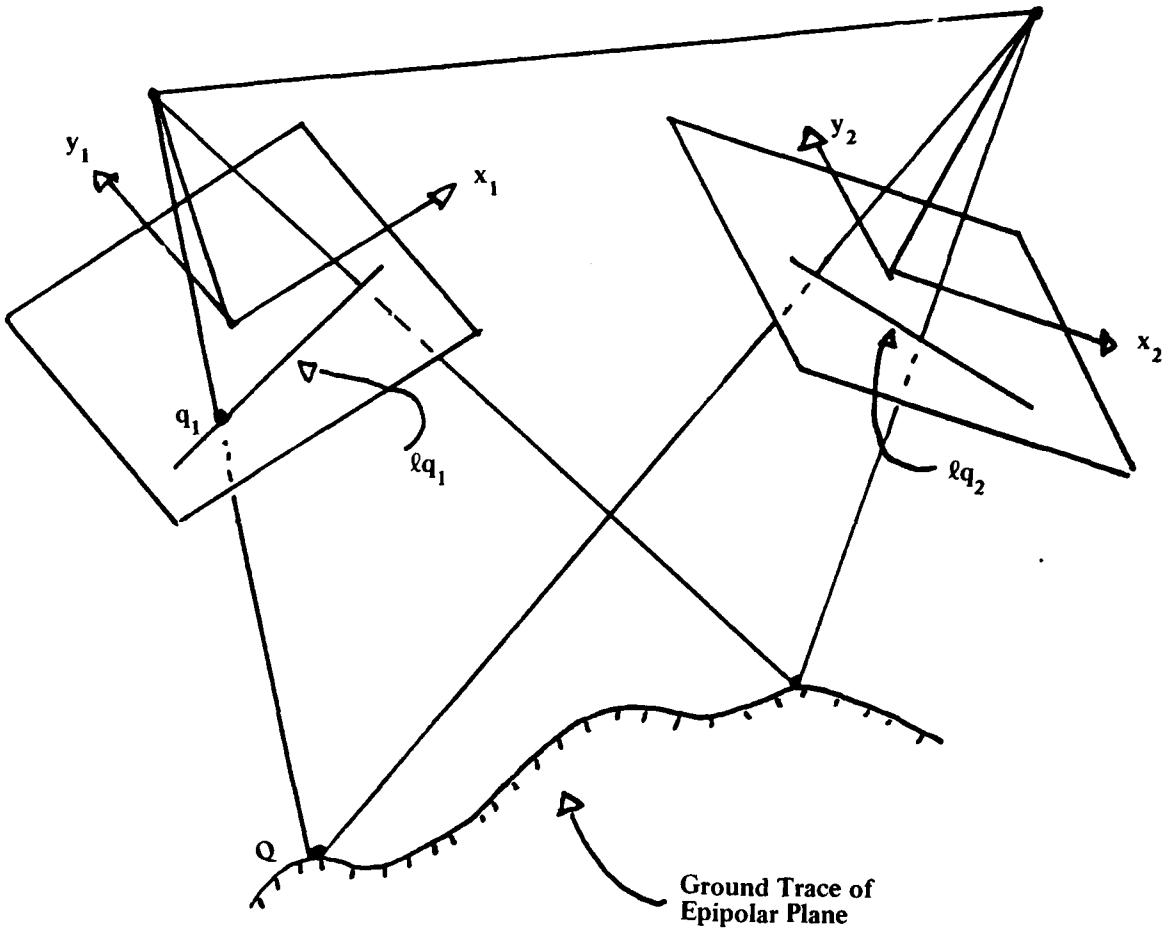

FIGURE 1. Epipolar Geometry.

If there is a fixed, or predictable, relative orientation between the two exposures, then the following relation holds:

$$C_p = P_1 X P_2 \cdot B = 0$$

The vectors $\bar{P}_2$ and $\bar{B}$ are functions of the relative orientation parameters and, along with $\bar{P}_1$, are described in appendix D. If the six relative orientation parameters defined in appendix D are known, or estimated, then the parameters plus any point, q_1 for example, will uniquely determine the epipolar lines ℓq_1 and ℓq_2. If the relative orientation data is correct, then any point on ℓq_2 along with q_1 (or any point on ℓq_1) will satisfy the vector equation given above.

To clarify some of the ideas with numerical examples, the author conducted the experiment described previously. It was assumed then that the relative orientation data was correct and that the scanned data was in fact epipolar data. Large line errors and large x–parallax errors were induced on the second image, and the line shifts were estimated using the ΔYp_2 correction given in appendix D. The results are listed in table 4 and show a close approximation to the induced errors.

Using the ΔYp_2 correction given in appendix D implies that the relative orientation parameters are correct and that the correct line is selected on the left image. In this instance, y–parallax is due entirely to not selecting the corresponding line on the right image. Effectively using the coplanarity condition equation requires that the acquisition system be under control and that the relative geometry for the stereo imaging system be considered. For example, consider Model 1 described in appendix A. In this model, the design relative orientation parameters are given below.

$$A_{21} = \begin{pmatrix} \text{Cos } 2\theta & 0 & \text{Sin } 2\theta \\ 0 & 1 & 0 \\ -\text{Sin } 2\theta & 0 & \text{Cos } 2\theta \end{pmatrix}$$

$$B = \begin{pmatrix} \delta x \\ o \\ -\delta x \text{ Tan } \theta \end{pmatrix}$$

where

θ : camera pitch

δx: x – component of relative baseline.

From appendix D,

$$J_1 = Yp_1 \delta x \, \mathrm{Tan}\theta \qquad X'p_2 = f \, \mathrm{Sin} \, 2\theta$$

$$J_2 = f\delta x \qquad Y'p_2 = Yp_2$$

$$J_3 = Yp_1 \delta x \qquad zp_2' = -f \, \mathrm{Cos} \, 2\theta$$

and

$$Cp = f\delta x (Yp_2 - Yp_1) = 0$$

f = camera focal length

Assume that an attempt will be made to maintain the fixed relative orientation of Model 1 over time. The following linear correction equation can be used to correct relative orientation whenever the relative orientation is sampled from exterior orientation data. Let the three fundamental angles of A_{21} be roll, pitch, and yaw (ω, ϕ, κ), then

$$\omega = 0$$

$$\phi = -2\theta$$

$$\kappa = 0$$

The linear correction equation is

$$\sum_{\xi} \frac{\partial Cp}{\partial \xi} \Delta \xi = -Cp$$

$$\xi = \delta x, \, \delta y, \, \delta z, \, \omega, \, \phi, \, \kappa$$

The coefficients of the corrections are obtained by a straightforward partial differentiation of the coplanarity relation with respect to the pertinent relative orientation parameters.

$$\frac{\partial Cp}{\partial \delta x} = f(Yp_2 - Yp_1 Cos\ 2\theta)$$

$$\frac{\partial Cp}{\partial \delta y} = f^2\ Sin\ 2\theta$$

$$\frac{\partial Cp}{\partial \delta z} = fYp_1\ Sin\ 2\theta$$

$$\frac{\partial Cp}{\partial \omega} = -\delta x\,(f^2 + Yp_1 Yp_2)$$

$$\frac{\partial Cp}{\partial \phi} = \delta x Yp_1\, f(Sin\ 2\theta + Tan\,\theta\ Cos\ 2\theta)$$

$$\frac{\partial Cp}{\delta \kappa} = \delta x\,(f^2\ Sin\ 2\theta + Yp_1 Yp_2\ Tan\,\theta)$$

Note that in Model 1 $Yp_1 = Yp_2$. Several detectors could be selected over the array to produce observation equations for input to a Kalman type filter for a sequential adjustment over time. Since the relative orientation parameters are themselves functions of exterior orientation parameters, the basic condition equation can be modified to reflect indirect observations on the exterior orientation data.

The same kind of analysis can be applied to the Model 2 acquisition system. There, several fixed relative orientations would be maintained since the desired relative orientation is a dynamic one.

CONCLUSIONS

1. Real time collection of elevation data using epipolar correlation techniques is not feasible.

2. A modification of the absolute difference measure of similarity should be evaluated to determine whether it provides a worthwhile improvement over the more conventional linear correlation measure.

3. Real time mensuration of y–parallax can be used as a means to help maintain a desired relative orientation in a variety of digital collection systems.

APPENDIX A.

Digital Stereo Model 1 ■ The sensor is defined to be a linear array of rectangular, solid-state detectors located f units (f ≈ focal distance of the lens) from the rear nodal point of the lens. The camera is regarded as a thin framelet as shown in figure A1.

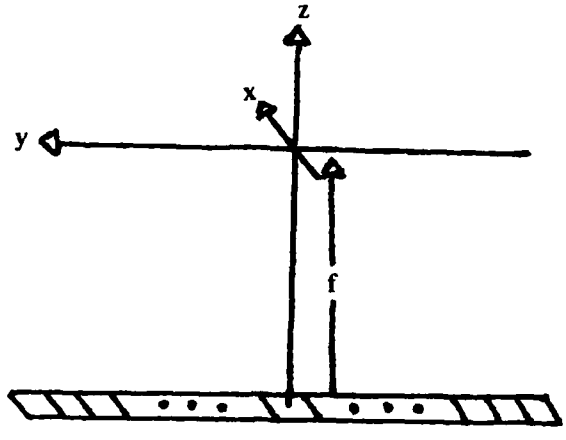

FIGURE A1. Model 1 Camera Coordinate Frame.

The origin of the camera coordinate frame is located at the rear nodal point of the lens, with the x–axis oriented toward the flight direction. The detectors are rectangular with dimensions Δx and Δy.

Model 1 is similar to a strip camera mode where a narrow slit is perpendicular to the flight direction and the film is moved past the slit at image point speed. Ground coverage is obtained by a moving vehicle whose velocity and flying height are used to determine the image point speed. Stereo ground coverage is obtained by employing two such systems in the vehicle where the optical axes are pitched toward one another. In the digital system, ground reflectance data is read out of the detectors and transmitted rather than recorded on film.

The forward camera of the stereo pair is described in figure A2.

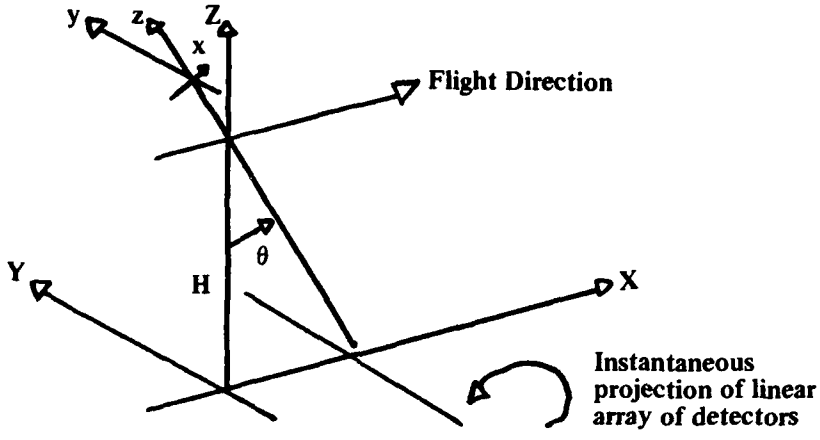

H: Flying height

θ: Camera Pitch

FIGURE A2. Model 1 Forward Camera.

The geometric relationship between points in the linear array and its projection on the X -plane is expressed by the following colinear relation:

$$\begin{pmatrix} xp \\ yp \\ -f \end{pmatrix} \; 1/\ell p \; = \begin{pmatrix} \text{Cos } \theta & 0 & \text{Sin } \theta \\ 0 & 1 & 0 \\ -\text{Sin } \theta & 0 & \text{Cos } \theta \end{pmatrix} \begin{pmatrix} Xp \\ Yp \\ -H \end{pmatrix} \; 1/Lp$$

where

$$\ell p = \sqrt{xp^2 + yp^2 + f^2}$$

$$Lp = \sqrt{Xp^2 + Yp^2 + H^2}$$

P is any point on the projection of the array.

The xp–coordinate is zero in this model. Line number (or exposure time) is used in place of y–coordinates. The ground dimensions of a projected detector (foot–print size) is computed next.

The image coordinates are derived directly from the colinearity model,

$$xp = f \frac{Xp \cos\theta - H \sin\theta}{Xp \sin\theta - H \cos\theta} = 0$$

$$\text{or} \qquad Xp = H \tan\theta$$

$$yp = \frac{f}{H} Yp \cos\theta$$

The footprint dimensions are obtained by differentiating the expressions for xp and yp, respectively, and then letting $Xp = H \tan\theta$.

$$\Delta X = H/f \sec^2\theta \Delta x$$

$$\Delta y = H/f \sec\theta \Delta y$$

The aft camera is essentially the same as the forward camera except that the pitch angle is in the opposite direction. The diagram in figure A3 is a profile of the two cameras when the same ground line is imaged.

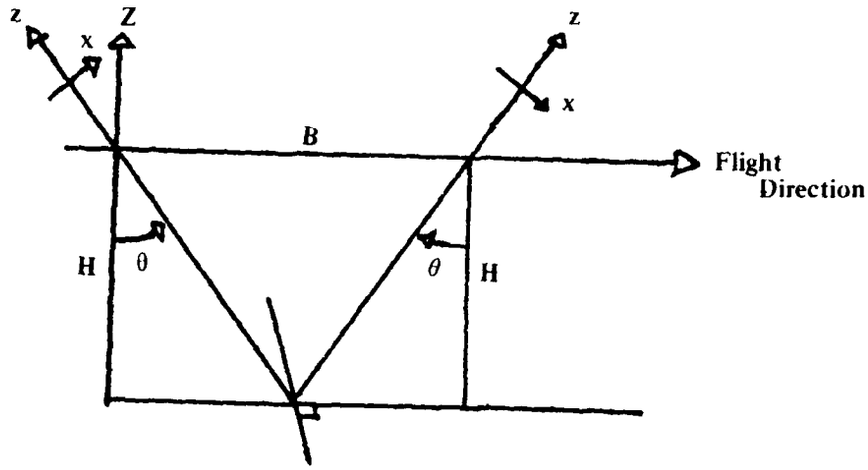

FIGURE A3. Model 1 Stereo Pair.

The base line distance $B = 2H \text{ Tan } \theta$ can be used to determine the model exposure interval if the vehicle speed V is known, i.e. $\Delta T = 2H/V \text{ Tan } \theta$. Note that since the projection of the linear array is perpendicular to the ground track,the output of the Jth detector on the forward camera and the output of the Jth detector on the aft for all exposures constitute an epipolar stream of reflectance values. This is true for all $J = 1, N$ detectors, as long as the relative geometry described above is maintained. If the relative geometry is maintained over time, then the Jth pixel at time T_1 on the forward array corresponds to the Jth pixel at time $(T_1 + \Delta T + \delta T)$ on the aft array. The time shift δT pertains to x-parallex because of an elevation value other than zero. The x-parallax is determined by correlation methods using the two sets of corresponding epipolar data sampled at the Jth detectors over time.

APPENDIX B.

Digital Stereo Model 2 ■ The sensor coordinate frame here is the same as in Model 1 except that the linear array of detectors is toward the flight direction (see figure B1).

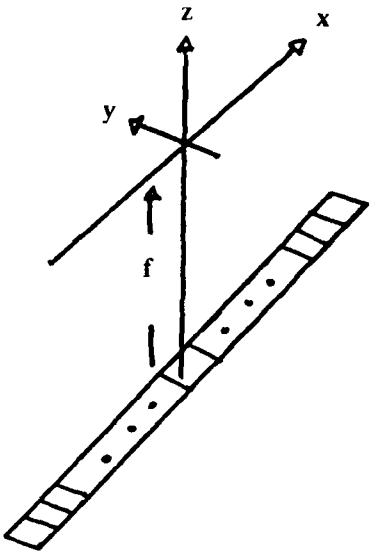

FIGURE B1. Model 2 Camera Coordinate Frame.

Model 2 is similar to a panoramic scanning mode where a narrow slit is arranged in the flight direction and the lens system is rotated across the flight path to acquire ground coverage. Again, as in the first model, stereo coverage is obtained by employing two such systems in the vehicle where, again, the optical axes are pitched toward one another. As before, digital data is read out of the detectors and transmitted rather than stored on film.

The forward camera of the stereo pair is described in figure B2.

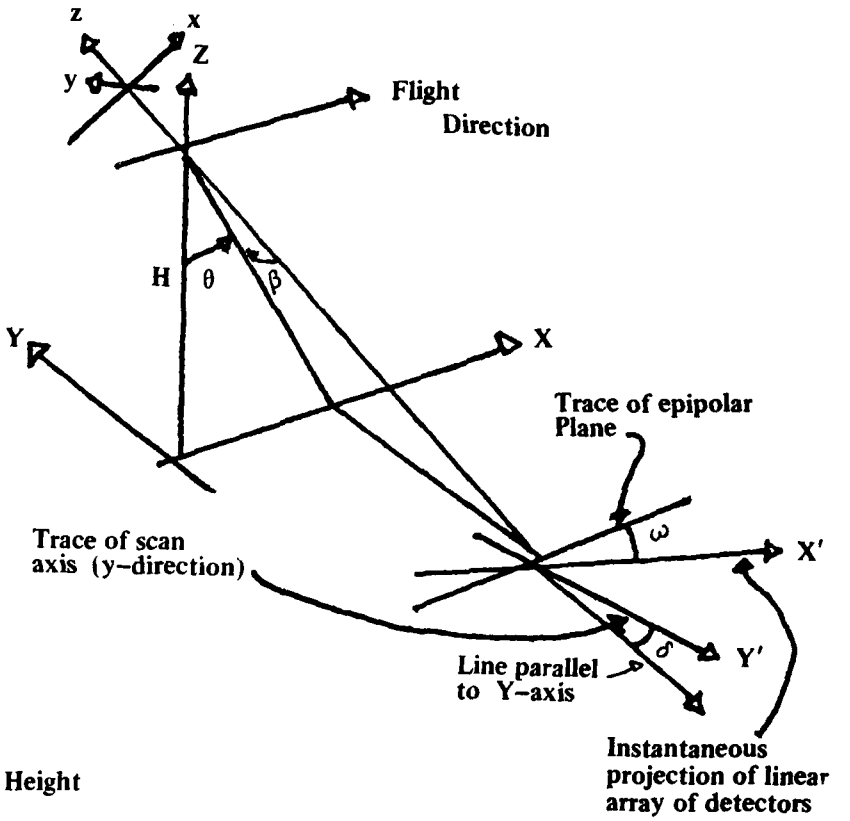

H: Flying Height

θ: Camera Pitch

β: Instantaneous Sweep Angle

FIGURE B2. Model 2 Forward Camera.

The relationship between points in the linear array and its projection in the XY–plane is expressed by the following colinear model:

$$\begin{pmatrix} xp \\ yp \\ -f \end{pmatrix} 1/\ell p = \begin{pmatrix} 1 & 0 & 0 \\ 0 & \text{Cos}\,\beta p & \text{Sin}\,\beta p \\ & -\text{Sin}\,\beta p & \text{Cos}\,\beta p \end{pmatrix} \begin{pmatrix} \text{Cos}\,\theta & 0 & \text{Sin}\,\theta \\ 0 & 1 & 0 \\ -\text{Sin}\,\theta & 0 & \text{Cos}\,\theta \end{pmatrix} \begin{pmatrix} Xp \\ Yp \\ -H \end{pmatrix} \quad 1/Lp$$

where

$$lp = (xp^2 + yp^2 + f^2)^{1/2}$$

$$Lp = (Xp^2 + Yp^2 + H^2)^{1/2}$$

P is any point

The instantaneous yp–coordinate is always zero in this mode since the linear array of detectors is regarded as a straight line in the focal plane. By setting yp = 0, the following pair of equations can be derived from the colinearity model:

$$xp = -f\text{Cos}\,\beta p \left(\frac{Xp\text{Cos}\,\theta - H\text{Sin}\,\theta}{-Xp\text{Sin}\,\theta - H\text{Cos}\,\theta} \right)$$

$$\beta p = \text{Tan}^{-1} \left(\frac{Yp}{Xp\text{Sin}\,\theta + H\text{Cos}\,\theta} \right)$$

and

$$Xp = -H \frac{xp\text{Cos}\,\theta + f\text{Sin}\,\theta\ \text{Cos}\,\beta p}{xp\text{Sin}\,\theta - f\text{Cos}\,\theta\ \text{Cos}\,\beta p}$$

$$Yp = -H \frac{f\text{Sin}\,\beta p}{xp\text{Sin}\,\theta - f\text{Cos}\,\theta\ \text{Cos}\,\beta p}$$

The angle ω is the angle between the epipolar plane trace in the XY–plane and the zx–plane trace in the XY–plane. It is assumed here that the flight path is parallel to the X–axis. The tangent of ω is $\frac{\partial Yp}{\partial Xp}$ where P is any point on the array (see figure B3).

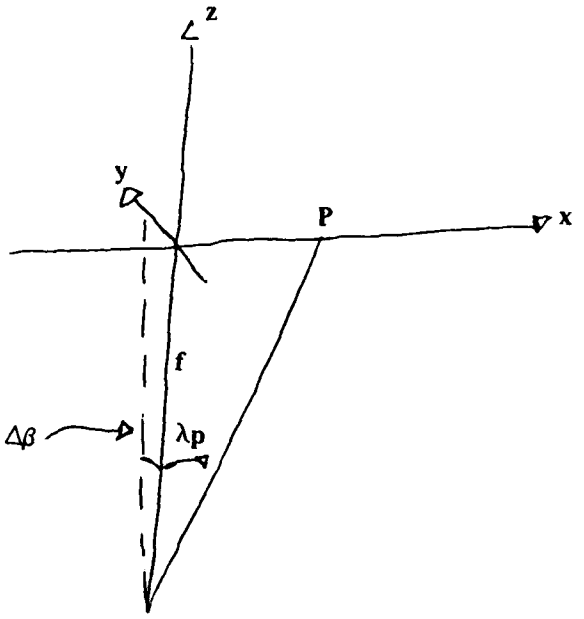

FIGURE B3. Model 2 Interior Geometry.

From the diagram, $xp = f \operatorname{Tan} \lambda p$, and from the ground point formulas,

$$\frac{\partial Y}{\partial \lambda p} = \frac{H \operatorname{Sin} \beta \operatorname{Sec}^2 \lambda p \operatorname{Sin} \theta}{(\operatorname{Tan} \lambda \, p \operatorname{Sin} \theta - \operatorname{Cos} \theta \operatorname{Cos} \beta)^2}$$

$$\frac{\partial X}{\partial \lambda p} = \frac{-H \operatorname{Sec} \lambda \, p \operatorname{Cos} \beta}{(\operatorname{Tan} \lambda \, p \operatorname{Sin} \theta - \operatorname{Cos} \theta \operatorname{Cos} \beta)^2}$$

$$\frac{\partial Y}{\partial X} = \frac{\dfrac{\partial Y}{\partial \lambda}}{\dfrac{\partial X}{\partial \lambda}} = \operatorname{Tan} \omega = -\operatorname{Tan} \beta \operatorname{Sin} \theta$$

The X' –footprint dimension along the projection of the linear array is computed next. From the relation $\mathrm{Tan}\,(\lambda+\Delta\lambda) = (x+\Delta x)/f$,

$$\Delta x \simeq \frac{f\mathrm{Sec}^2\,\lambda\,\Delta\lambda}{1-\Delta\lambda\,\mathrm{Tan}\,\lambda}$$

and

$$\Delta\lambda \simeq \frac{\Delta x}{f\mathrm{Sec}^2\,\lambda+\Delta x\,\mathrm{Tan}\,\lambda}$$

The rate of change of X with respect of x is

$$\frac{\partial X}{\partial x} = \lim_{\Delta x\to 0}\frac{\Delta X}{\Delta x} = \lim_{\Delta x\to 0}\frac{\frac{\partial X}{\partial\lambda}}{\frac{\partial x}{\partial\lambda}} = -\frac{H\mathrm{Sec}^2\,\lambda\,\mathrm{Cos}\,\beta}{\frac{(\mathrm{Tan}\,\lambda\,\mathrm{Sin}\,\theta-\mathrm{Cos}\,\theta\,\mathrm{Cos}\,\beta)^2}{f\mathrm{Sec}^2\,\lambda}}$$

$$= -\frac{H}{f}\,\frac{\mathrm{Cos}\,\beta}{(\mathrm{Tan}\,\lambda\,\mathrm{Sin}\,\theta-\mathrm{Cos}\,\theta\,\mathrm{Cos}\,\beta)^2}$$

Let $\frac{\partial X'}{\partial x}$ be the rate of change along the array projection, then

$$\frac{\partial X'}{\partial x} = \frac{\partial X}{\partial x}\Big/\mathrm{Cos}\,\omega = -\frac{H}{f}\,\frac{\mathrm{Cos}\,\beta\sqrt{1+\mathrm{Sin}^2\,\theta\,\mathrm{Tan}^2\,\beta}}{(\mathrm{Cos}\,\theta\,\mathrm{Cos}\,\beta-\mathrm{Tan}\,\lambda\,\mathrm{Sin}\,\theta)^2}$$

then the X-footprint dimension is

$$\Delta X' = \frac{H}{f}\,\frac{\mathrm{Cos}\,\beta\sqrt{1+\mathrm{Sin}^2\,\theta\,\mathrm{Tan}^2\,\beta}}{(\mathrm{Cos}\,\theta\,\mathrm{Cos}\,\beta-\mathrm{Tan}\,\lambda\,\mathrm{Sin}\,\theta)^2}\,\Delta x$$

The Y'-footprint dimensions along the projection of the scan axis is computed next. The projection angle δ is computed in the following way:

$$\text{Tan}\,\delta = \frac{\frac{\partial X}{\partial \beta}}{\frac{\partial Y}{\partial \beta}}$$

$$\frac{\partial X}{\partial \beta} = \frac{H \,\text{Tan}\,\lambda \,\text{Sin}\,\beta}{(\text{Tan}\,\lambda \,\text{Sin}\,\theta - \text{Cos}\,\theta \,\text{Cos}\,\beta)^2}$$

$$\frac{\partial Y}{\partial \beta} = \frac{H\,(\text{Cos}\,\theta - \text{Tan}\,\lambda \,\text{Sin}\,\theta \,\text{Cos}\,\beta)}{(\text{Tan}\,\lambda \,\text{Sin}\,\theta - \text{Cos}\,\theta \,\text{Cos}\,\beta)^2}$$

and

$$\text{Tan}\,\delta = \frac{\text{Tan}\,\lambda \,\text{Sin}\,\beta}{\text{Cos}\,\theta - \text{Tan}\,\lambda \,\text{Sin}\,\theta \,\text{Cos}\,\beta}$$

$$\text{Cos}\,\delta = \frac{1}{\sqrt{\frac{1 + \text{Tan}^2\,\lambda \,\text{Sin}^2\,\beta}{(\text{Cos}\,\theta - \text{Tan}\,\lambda \,\text{Sin}\,\theta \,\text{Cos}\,\beta)^2}}}$$

$$\frac{\partial Y}{\partial y} = \frac{\partial Y}{\partial \beta}\,\frac{\partial \beta}{\partial y} = \frac{H}{f}\left[\frac{\text{Cos}\,\theta - \text{Tan}\,\lambda \,\text{Sin}\,\theta \,\text{Cos}\,\beta}{(\text{Tan}\,\lambda \,\text{Sin}\,\theta - \text{Cos}\,\theta \,\text{Cos}\,\beta)^2}\right]$$

$$\frac{\partial Y}{\partial y} = \frac{\partial Y'}{\partial y}\Big/\text{Cos}\,\delta = \frac{H}{f}\left\{\frac{\sqrt{(\text{Cos}\,\theta - \text{Tan}\,\lambda \,\text{Sin}\,\theta \,\text{Cos}\,\beta)^2 + \text{Tan}^2\,\lambda \,\text{Sin}^2\,\beta}}{(\text{Tan}\,\lambda \,\text{Sin}\,\theta - \text{Cos}\,\theta \,\text{Cos}\,\beta)^2}\right\}$$

Then the Y-footprint dimension is

$$\Delta Y' = \frac{H}{f}\,\frac{\sqrt{(\text{Cos}\,\theta - \text{Tan}\,\lambda \,\text{Sin}\,\theta \,\text{Cos}\,\beta)^2 + \text{Tan}^2\,\lambda \,\text{Sin}^2\,\beta}}{(\text{Tan}\,\lambda \,\text{Sin}\,\theta - \text{Cos}\,\theta \,\text{Cos}\,\beta)^2}\,\Delta y$$

The aft camera is essentially the same as the forward camera except that the pitch angle is in the opposite direction. Note that the epipolar trace is parallel to the ground X–axis, but because of the pitch, the projection of the array is not parallel to the epipolar trace. Furthermore, the projection of the aft array for the same sweep angle β also makes an angle ω with respect to the epipolar trace, but in the opposite direction. This means that there is a relative skew between forward and aft data and that the skew varies with β. It is shown below that the relative skew in the image domain is not 2ω. In fact, because of the scan procedure, the focal plane must be regarded as a section of a cylinder. As a result, the projection of the epipolar trace onto the cylindrical focal plane is not even a straight line.

The equation for the projection of the epipolar trace onto the cylindrical focal plane is derived in appendix C. Assume for the present that the cone angle of the camera is small enough so that the curved line can be approximated by a straight line. The slope of the approximate straight line is computed next.

The slope of the projection of the epipolar trace with respect to the camera x–axis at xp = 0 is K where

$$\text{TanK} = \frac{\partial y}{\partial x} = \frac{\frac{\partial y}{\partial X}}{\frac{\partial x}{\partial X}}$$

From the colinearity relations,

$$\frac{\partial x}{\partial X} = \frac{fH\text{Cos}\,\beta}{(X\text{Sin}\,\theta + H\text{Cos}\,\theta)^2}$$

$$\frac{\partial y}{\partial X} = \frac{\partial y}{\partial \beta}\,\frac{\partial \beta}{\partial X} = -\frac{fY\text{Sin}\,\theta\,\text{Cos}^2\,\beta}{(X\text{Sin}\,\theta + H\text{Cos}\,\theta)^2}$$

$$\frac{\partial y}{\partial \beta} = f$$

$$\frac{\partial\beta}{\partial x} = \frac{-Y\text{Sin}\,\theta\,\text{Cos}^2\,\beta}{(X\text{Sin}\,\theta + H\text{Cos}\,\theta)^2}$$

then

$$\text{TanK} = \frac{-Y}{H}\ \text{Sin}\,\theta\,\text{Cos}\,\beta$$

and from the colinearity relations,

$$Y(xp = 0) = \frac{H\text{Sin}\,\beta}{\text{Cos}\,\theta\,\text{Cos}\,\beta}$$

and finally

$$\text{TanK} = -\text{Tan}\,\theta\,\text{Sin}\,\beta$$

Epipolar data cannot be extracted from corresponding pixels over time when Model 2 is used. In fact, a complex sampling procedure requiring expensive buffer storage must be developed if epipolar data is processed in flight. This problem can be eased if one more degree of freedom is introduced into the scan procedure. If the optical axis of the rotating camera is yawed by an angle $K = \text{Tan}^{-1}(-\text{Tan}\,\theta\,\text{Sin}\,\beta)$ during scan, then the projection of the epipolar trace will be coincident with the linear array. Image data from the forward and aft cameras, for the same sweep angle, will be corresponding epipolar data.

There is still the problem of collecting epipolar data from the forward and aft cameras in a practical manner. If the two cameras are rotated in the same direction so that the sweep angles are identical for a given time, then epipolar data can be processed when collected. Such a scan procedure will introduce a vehicle rotational effect that must be countered. If the two cameras are rotated in opposite directions so that, for example, both view the nadir epipolar trace at the same time, then the vehicle rotational effect is cancelled, but corresponding epipolar lines of data off ground nadir are collected at dirrerent times. This introduces storage problems for near real time processing.

APPENDIX C. Equation of Epipolar Trace on Cylindrical Focal Plane •

Assume that the stereo model is as defined in appendix B, then from the colinearity relations

$$Y \operatorname{Cot} \beta = X \operatorname{Sin} \theta + H \operatorname{Cos} \theta$$

or

$$X = Y \operatorname{Csc} \theta \operatorname{Cot} \beta - H \operatorname{Cot} \theta$$

Substitute this expression for X into the first of the colinearity equations, and after some algebraic simplication, the result is

$$\frac{Y}{f} \operatorname{Sin} \theta \, x + H \operatorname{Sin} \beta = Y \operatorname{Cos} \theta \operatorname{Cos} \beta$$

Note that if an xy–coordinate frame is defined on the cylindrical section, then $y = f^{*}\beta$ or $\beta = y/f$. The objective here is to square the above equation and solve the resulting quadratic equation for Sin β. The result, after some algebraic simplication is

$$\operatorname{Sin} \beta = - \frac{\frac{x Y H \operatorname{Sin} \theta}{f} + Y \operatorname{Cos} \theta \sqrt{Y^2 \operatorname{Cos}^2 \theta + H^2 - \frac{x^2 Y^2}{f^2} \operatorname{Sin}^2 \theta}}{H^2 + Y^2 \operatorname{Cos}^2 \theta}$$

and finally

$$y = f \operatorname{Sin}^{-1} \left\{ \frac{Y \cos \theta \sqrt{Y^2 \operatorname{Cos}^2 \theta + H^2 - \frac{x^2 Y^2 \operatorname{Sin}^2 \theta}{f^2}} - \frac{xYH \operatorname{Sin}^2 \theta}{f}}{H^2 + Y^2 \operatorname{Cos}^2 \theta} \right\}$$

The projection of the epipolar trace onto the cylindrical focal plane is described in figure C1.

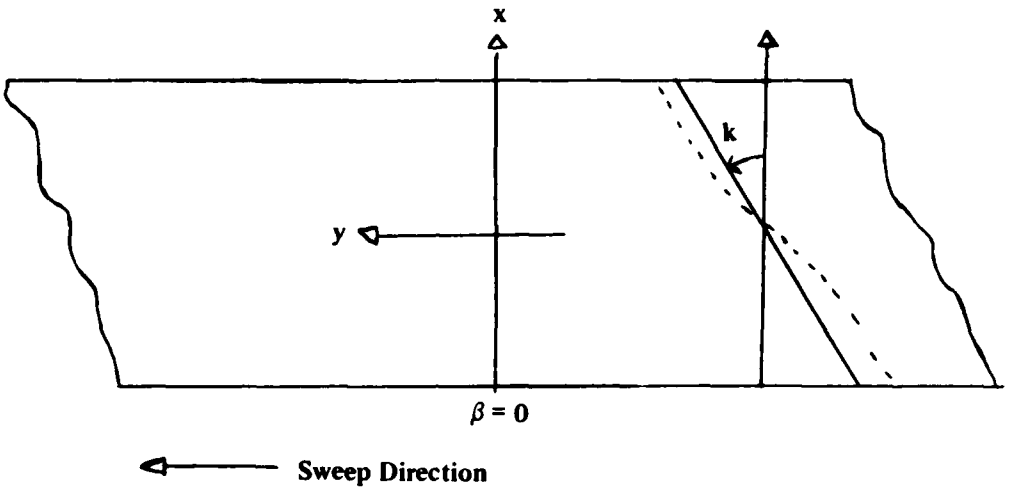

Approximate Epipolar Line: _____

Exact Epipolar Line: - - - - - - -

FIGURE C1. Epipolar Line.

The difference between the exact and approximate epipolar lines is greatly exaggerated in the diagram. Consider the following example where the pitch is $\theta = 10°$ and where $|x/f| < 0.1$. This example provides a forward field of view of 11.42°. Let $\beta = -30°$ then $K = 5.038°$. If the focal length is 30 inches (76cm), then $|x| < 3.0$ inches (7.6cm) and the exact epipolar line is expressed in table C1. Note that the second differences are insignificant, which means that the y-values can be represented as a linear function of the x-values.

$$y = -15.70796331 + x * \text{Tan } K$$

or

$$y = -15.70796331 + 0.088163490 * x$$

TABLE C1. Epipolar Line Example.

x	y	Δy	$\Delta^2 y$
-3.0	-15.97245721		
-2.4	-15.91955744	.05289977	
-1.8	-15.86665834	.05289910	-.00000067
-1.2	-15.81375972	.05289862	-.00000048
-0.6	-15.76086114	.05289828	-.00000034
0.0	-15.70796331	.05289813	-.00000015
0.6	-15.65506518	.05289813	.0
1.2	-15.60216691	.05289827	.00000014
1.8	-15.54926829	.05289862	.00000035
2.4	-15.49636919	.05289910	.00000048
3.0	-15.44346942	.05289977	.00000067

$\theta = 10°$

$\beta = -30°$

$f = 30''$

APPENDIX D.

Coplanarity Condition Equation ■ The coplanarity condition requires that the base line between lens positions of two exposures and the two imaging rays of a common ground point be coplanar. The relevant geometry is shown in figure D1.

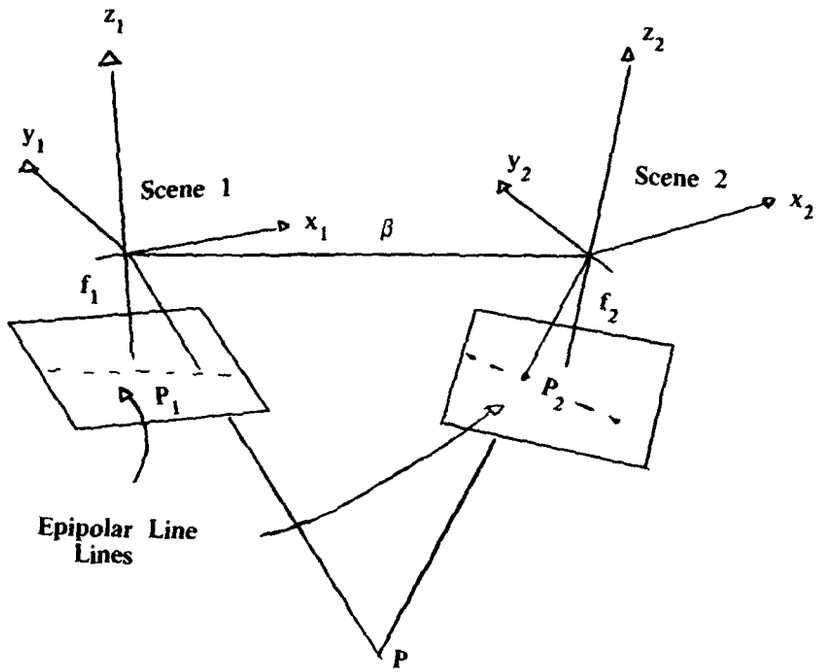

FIGURE D1. Relative Geometry.

Define A_{21} as the (3 x 3) rotation matrix that relates directions in scene 2 to directions in scene 1. Express the two imaging rays $\bar{p}_1$ and $\bar{p}_2$ in scene 1.

$$P_1 = \begin{pmatrix} xp_1 \\ yp_1 \\ -f_1 \end{pmatrix} \quad ; \quad P_2 = A_{21} \begin{pmatrix} xp_2 \\ yp_2 \\ -f_2 \end{pmatrix} = \begin{pmatrix} x' \; p_2 \\ y' \; p_2 \\ z' \; p_2 \end{pmatrix}$$

Define the baseline vector $\bar{B}$ as a set of direction numbers describing the direction of lens 2 from lens 1 in scene 1.

$$\bar{B} = \begin{pmatrix} \delta x \\ \delta y \\ \delta z \end{pmatrix}$$

If the two imaging vectors $\bar{P}_1$ and $\bar{P}_2$ are to intersect at P, then $\bar{B}$, $\bar{P}_1$, and $\bar{P}_2$ must be coplanar. Coplanarity is assured if the following vector equation is satisfied:

$$Cp = \bar{P}_1 \times \bar{P}_2 \bullet \bar{B} = 0$$

If Cp is expanded, then the equation takes the form

$$Cp = J_1 x' p_2 + J_2 y' p_2 + J_3 z' p_2 = 0$$

$$J_1 = -f_1 \delta y - yp_1 \delta z$$

$$J_2 = f_1 \delta x + xp_1 \delta z$$

$$J_3 = yp_1 \delta x - xp_1 \delta y$$

The rotation matrix A_{21} can be uniquely defined by three angles α_1, α_2, and α_3. It can be shown that only five of the six relative orientation parameters (δx, δy, δz, α_1, α_2, α_3) are independent, that is,one of the six parameters must be held constant. Note that the coplanarity condition is independent of the ground point P. The condition requires only that the three vectors B, $\bar{P}_1$, and $\bar{P}_2$ be coplanar. For example, if errors in xp_1, xp_2, or both are made along their respective epipolar lines (x–parallax errors), then the coplanarity condition is unaffected. However, errors in y (y–parallax errors) are readily detected.

If, for example, the relative orientation data is held constant along with (xp_1, yp_1), then the y–parallax error is

$$\Delta yp = -Cp/(a_{12} J_1 + a_{22} J_2 + a_{32} J_3)$$

where a_{ij} are from A_{21}.

In general, corrections to the four coordinates can be obtained by a Taylor expansion about the four coordinates and retaining only the constant and first order terms.

$$Cp + \frac{\partial Cp}{\partial xp_1} \Delta xp_1 + \frac{\partial Cp}{\partial yp_1} \Delta yp_1 + \frac{\partial Cp}{\partial xp_2} \Delta yp_2 + \frac{\partial Cp}{\partial yp_2} \Delta yp_2 = 0$$

where

$$\frac{\partial Cp}{\partial xp_1} = \delta zy' \; p_2 - \delta y \; z' \; p_2$$

$$\frac{\partial Cp}{\partial yp_1} = \delta X \; z' \; p_2 - \delta zx' \; p_2$$

$$\frac{\partial Cp}{\partial xp_2} = a_{11} J_1 + A_{21} J_1 + a_{31} J_3$$

$$\frac{\partial Cp}{\partial yp_2} = a_{12} J_1 + a_{22} J_2 + a_{32} J_3$$

APPENDIX E.

Epipolar Correlation ■ Epipolar correlation pertains to one–dimensional image matching along corresponding lines of data over which y–parallax does not exist. Epipolar data is generated by a member of the family of planes, each member having as a common element the straight line connecting two or more exposure stations. Consider two overlapping frame camera exposures. An epipolar line pair results from the intersection of the associated epipolar plane and the two focal planes. An example of this geometry is presented in figure D1. In that example, the epipolar plane is defined by the baseline vector B and the ground point P.

Model 2, described in appendix B, produces curved epipolar lines that in most practical cases can be approximated by straight lines. An example of this geometry is presented in figure C1. Model 1, described in appendix A, produces streams of epipolar data collected over time from corresponding detectors.

Since epipolar data is derived from imagery defined by a plane containing the photographic base line, then all corresponding points satisfy the coplanarity condition equation described in appendix C. As a result, there is no y–parallax associated with such data. In fact, any pair of points, one point from the first line and the other any point from the second line, will satisfy the coplanarity relation. There is no analytical condition equation that will produce corresponding points along the epipolar pair of lines, because the relative positions of corresponding image points are directly related to unknown terrain elevations. Numerical correlation techniques are used to remove x–parallax or to determine corresponding points on epipolar line pairs.

The match process employed in this study is described next. One of the basic notions is that the match process is a refinement process rather than a search process. Regularly spaced image data is selected from the first line, and the second line is "shaped" to reflect the expected x–parallax. Shaping is accomplished by using results from a previously matched, nearby line pair, that is, the spacings of corresponding points along the second line are assumed to be exactly like those of the previous second line. Every possible point is matched by developing a set of correlation functions and determining their maximal points. Three measures of similarity are evaluated in this study to develop the correlation functions.

$$XDY = \sum^{n} |X - Y|$$

$$SXY = \sum^{n} (X - \bar{Y})\ (Y - \bar{Y})$$

$$RXY = SXY/(SX*SY)$$

$$\bar{X} = \frac{1}{n} \sum^{n} X$$

$$\bar{Y} = \frac{1}{n} \sum^{n} Y$$

$$SX = \sqrt{\sum^{n} (X - \bar{X})^2}$$

$$SY = \sqrt{\sum^{n} (Y - \bar{Y})^2}$$

X: Digital image data from the first line.

Y: Digital image data from the second line.